Scripta Materialia 112 (2016) 32–36

Contents lists available at ScienceDirect

Scripta Materialia

journal homepage: www.elsevier.com/locate/scriptamat

Nature of delamination cracks in pearlitic steels

Masaki Tanaka *, Hayato Saito, Motoki Yasumaru [1], Kenji Higashida

Department of Materials Science and Engineering, Kyushu University, 744 Motooka, Nishi-ku, Fukuoka, Fukuoka 819-0395, Japan

ARTICLE INFO

Article history:
Received 2 July 2015
Received in revised form 2 September 2015
Accepted 2 September 2015
Available online 18 September 2015

Keywords:
Severe plastic deformation (SPD)
Grain refining
Fracture
Mechanical property
Eutectic steel

ABSTRACT

Wire-drawn fully pearlitic steel was twisted at room temperature. As a result, a delamination crack propagated along the longitudinal direction of the wire. Backscattered electron and transmission electron microscopy images indicated that the cementite lamellae beneath the delamination crack had vanished. In addition, a fine-grained structure was observed. This indicated that the delamination fracture was not a brittle one but a shear one associated with local severe plastic deformation.

Pearlitic steels, which consist of lamellar structures of ferrite and cementite, can be readily drawn into wires. The ultimate tensile strength of pearlitic steels can be as high as 6.35 GPa in the case of specimens wiredrawn at a true strain of 6.02 [1]. Further, the lamellar structures of ferrite and cementite improve work hardening, owing to the transference of loads from the ferrite phase to the cementite phase [2,3]; the cementite layers bear much higher stresses than the ferrite ones do. However, one of the issues limiting the use of high-strength pearlitic steels is the onset of delamination during torsion. Delamination is a fracture phenomenon in which cracks propagate along the longitudinal direction of a wire during the process of torsion. Several mechanisms have been proposed to explain the onset of delamination. One is the effect of carbon dissolution during the wire-drawing process. It has been reported that cementite deforms during wire-drawing and that it undergoes decomposition in heavily drawn wires [4–9]. Li et al. [10] obtained the pearlitic steel with the tensile strength of 7 GPa, stabilising nanoscaled ferrite subgrains structure with supersaturating carbon dissolved from carbides. The decomposition of cementite results in the ferrite phase becoming supersaturated with carbon; this leads to inhomogeneities in the local strength. It is believed that the areas where a local change in strength occurs, that is, the regions with a relatively low strength, are the initiation sites of delamination cracks. The other works in the fracture mechanics-based viewpoint is that the delamination cracks are brittle fractures [11]. However, it remains unknown whether the delamination of pearlitic steel is a low-temperature embrittlement phenomenon or a ductile fracture associated with plasticity. Therefore, it is essential to first elucidate the phenomenon of delamination crack formation as well as the microstructures around such cracks, if one wishes to understand the mechanism responsible for the delamination of wire-drawn pearlitic steels. In the present study, we examined a delamination crack introduced by a torsion test and found that the delamination crack was associated with a local thin layer of severe plastic deformation immediately beneath the delamination crack.

The fully pearlitic steel SWRS82B was used in this study. A hot-rolled rod of the steel with a diameter of 9 mm was drawn to a diameter of 3 mm; the true strain in the latter case was 2.2. The 3-mm-diameter wire was then aged at 423 K for 3.6 ks. Next, 150 mm of the drawn wire was twisted by 360° at room temperature. We have performed several torsion tests and found that the onset of delamination crack is a scattered phenomenon. It is probably the inhomogeneity of microstructure of the specimen. A delamination crack was introduced during the torsion test. The drawn wire was then cut at the centre, and the microstructure beneath the delamination crack was observed. In addition to the torsion test, a simple shear test was also performed on the steel. A $3 \times 15 \times 0.6$ mm^3 plate with slits was cut from the centre of the dawn wire before the torsion test. The cross-head speed was set at 15 μm/min. The specimen was subjected to the shear strain until it fractured. Next, the fracture specimen was polished approximately 200 μm depth and observed by using a scanning electron microscope (SEM) (Zeiss Ultra-55). The microstructure beneath the delamination crack was also observed using a transmission electron microscope (TEM) (JEOL JEM-ARM200F).

Fig. 1(a) shows a backscattered electron (BSE) image of the longitudinal section of the hot-rolled specimen. The colony size in the hot-rolled specimen is approximately 5 μm. The areas with black and white contrasts represent the local differences in the crystallographic orientation. The average spacing of the cementite lamellae was approximately 150 nm, as measured at the edges of the lamellae. Fig. 1(b) shows an

* Corresponding author.
E-mail address: masaki@zaiko.kyushu-u.ac.jp (M. Tanaka).
[1] Present address: Denso Corp., 1-1 Showa-cho, Kariyashi, Aichi, 448-8661, Japan.

http://dx.doi.org/10.1016/j.scriptamat.2015.09.004
1359-6462/

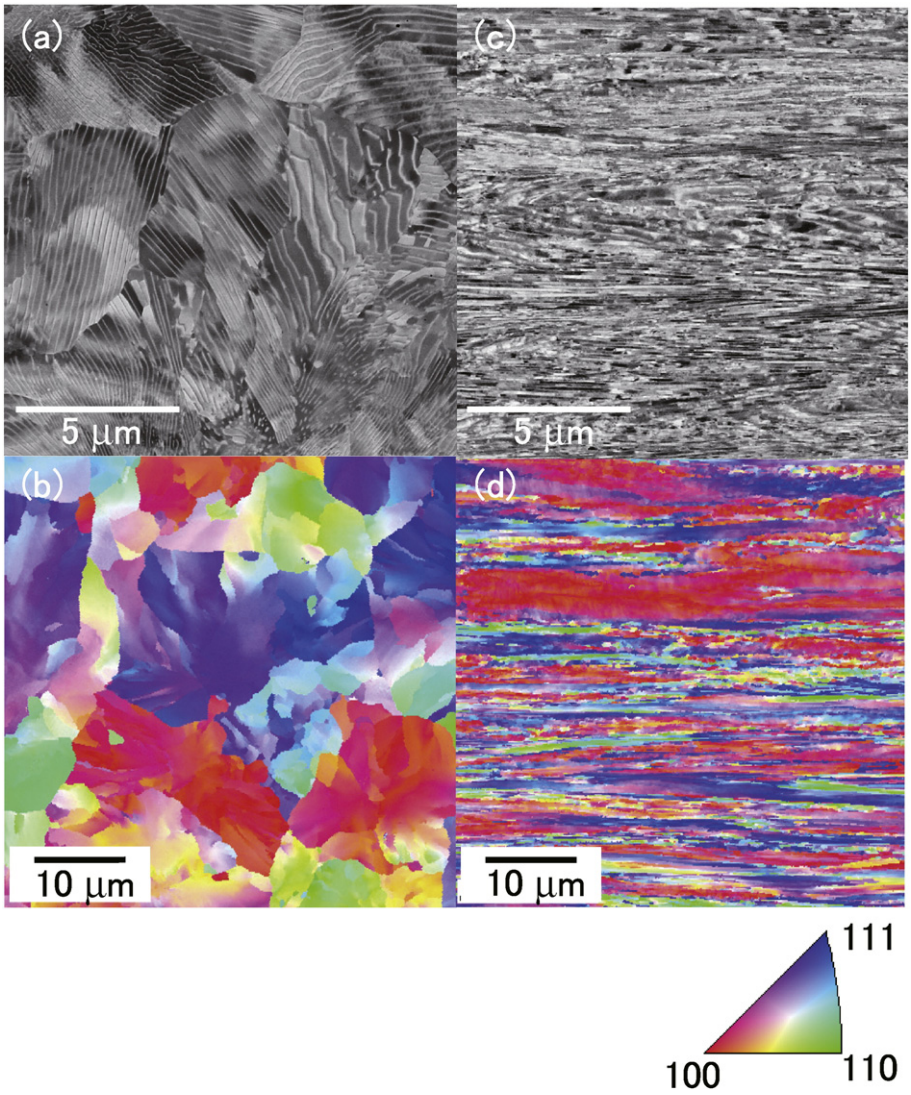

Fig. 1. Backscattered images and IPF maps of the longitudinal sections of the steel specimens tested. (a) and (b) are from a hot-rolled specimen and (c) and (d) are from a wire-drawn specimen.

inverse pole figure (IPF) map of the normal direction (ND) to the longitudinal section of the hot-rolled specimen. The block size is approximately 5 - 15 μm, and the blocks are homogeneously distributed. There are slight differences in the orientation within the blocks [12]; these correspond to the differences in contrast seen in (a). Fig. 1(c) shows a BSE image of the longitudinal section of the wire-drawn specimen. The cementite/ferrite lamellae are elongated along the drawing direction, which is horizontal in the figure. The lamellar spacing is lower and approximately 40 nm. Further, the individual blocks are no longer distinguishable. Fig. 1(d) shows an IPF map taken along the ND to the longitudinal section of the wire-drawn specimen. Although several blocks with widths of more than 5 μm are along the perpendicular direction, most of the blocks are segmented to submicrons. Next, in order to investigate the phenomenon of delamination in the wire-drawn specimen, a torsion test was performed on the specimen.

A delamination crack was observed propagating along the longitudinal direction of the wire after one rotation. This indicated that the delamination crack was initiated very early during twisting as a mode II crack along the longitudinal direction. Fig. 2(a) shows the cross-section at the centre of the wire-drawn specimen after one rotation. The crack trace at the cross-section lies at the centre of the wire. The delamination crack propagated both in the longitudinal direction and at the centre of the wire. Fig. 2(b) shows an SEM image of the fractured surface of the delamination crack indicated by an arrow in Fig. 2(a). The surface is very flat and smooth and there are no shear dimples, in contrast to what is seen in the case of ductile fractured surfaces. Fig. 2(c) shows the fracture surface of a specimen fractured at 120 K during an impact test; the surface exhibits characteristics of low-temperature embrittlement. The morphology of the surface in Fig. 2(b) is quite different from that of the surface in Fig. 2(c). Thus, it can be concluded that delamination cracks are not caused by low-temperature embrittlement. If the delamination crack were due to the result of simple ductile fracture, elongated dimples should have been observed. Flat surfaces without dimples or reviver patterns observed in this study indicate that they are neither a kind of simple ductile fracture surfaces nor cleavage ones. It is to be noted that the similar fracture surface was also seen in hydrogen embrittlement [13], where fracture surface appears flat in low resolution but was decollated fine-scale undulation. TEM observation immediately beneath the fracture surface elucidated dense arrangement of dislocations. This similarity of fracture surfaces between cracks of delamination and hydrogen embrittlement suggests that when dislocations are locally active immediately beneath the crack, fracture surface tends to be flat. The fracture mode observed here cannot be simply identified to be “ductile” or “brittle”.

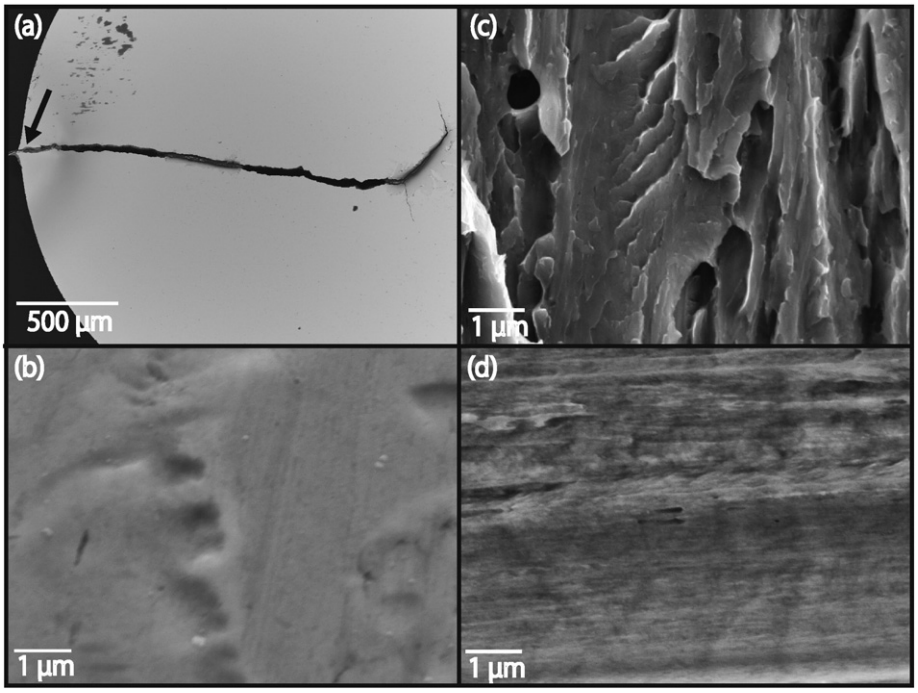

Fig. 2. (a) Cross section of a wire-drawn specimen after a torsion test. A delamination crack that extends from the surface to the centre of the wire can be seen. The crack propagated during rotation by 360° at room temperature. (b) SEM image of the fracture surface of the delamination crack. (c) SEM image of the surface of a specimen fractured at 120 K during an impact test. (d) SEM image of the fracture surface of a shear crack introduced during a simple shear test.

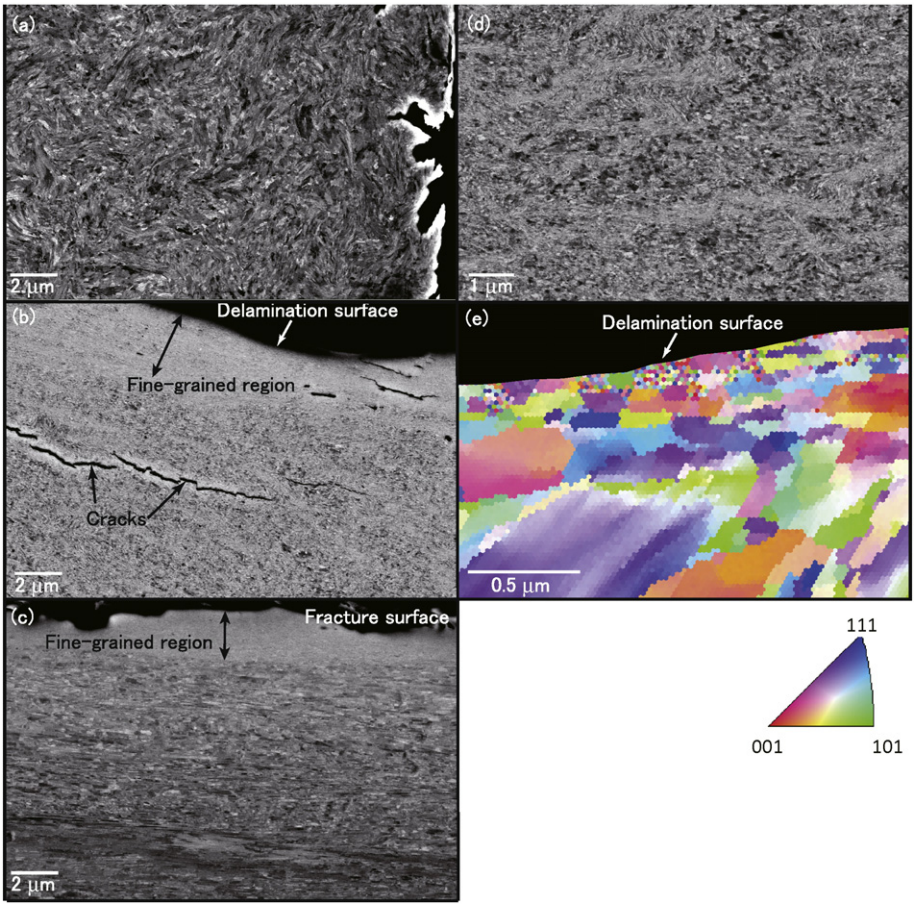

Fig. 3. (a) Cross-section of a wire-drawn specimen before the torsion test. (b) Cross-section of the wire-drawn specimen showing the area beneath the delamination crack after a torsion test. Fine grains can be seen beneath the crack. (c) Cross-sectional image of the area beneath the fracture surface of a specimen subjected to a simple shear test. Fine grains can be seen beneath the crack in this case too (d) Magnified image of the area near the delamination crack. This area is not the same as that in (b). (e) Inverse pole figure of normal direction immediately beneath the main delamination crack.

Further, assuming that delamination cracks are mode II cracks, the fracture surface in Fig. 2(a) should have been similar to that of a specimen subjected to simple shear cracking. Thus, a simple shear test was performed next, in order to compare the morphologies of the fracture surfaces of the delamination crack and the simple shear crack. Fig. 2(d) shows the fracture surface of the wire-drawn specimen subjected to a simple shear test. This surface is also flat and smooth. Further, neither shear dimples nor river patters can be seen on the fracture surface although it is slightly rougher than that of the delamination crack. Thus, it can be concluded that delamination cracks are similar to shear cracks of pearlitic steels. Therefore, in order to elucidate the nature of delamination cracks further, the side surfaces around the delamination crack as well as the shear crack were observed from the cross section of the wire.

Fig. 3(a) shows a BSE image of the cross-section of a wire-drawn specimen before the torsion test. Although the lamellae are bent when seen from this direction, the lamellar structure itself is still maintained. Fig. 3(b) shows a magnified image of the area around the delamination crack where the arrow shows in Fig. 2(a). The delamination crack is at the top of the figure. In this case, the lamellar structures are not as clear as those in Fig. 3(a). We would like to stress that, at a depth of 4 μm beneath the delamination crack, the lamellar structure disappeared. Further, the blocks at this depth were ultra-fined. It is also confirmed by using EBSD. Fig. 3(e) shows an inverse pole figure immediately beneath the delamination crack. The colour map shows the orientation of ferrite, indicating the smaller block size the nearer delamination surface. These results indicated that the local region under the delamination crack undergoes severe plastic deformation. That is to say, delamination cracks are not brittle cracks but are coincide with plastically deformed coinciding with severe plastic deformation. Since the grains immediately beneath the delamination crack are ultra-fined, it was not possible to determine the relationship between the delamination crack and crystallographic orientation of slip planes. Fig. 3(c) shows a BSE image of the area beneath the shear crack shown in Fig. 2(d); this crack was formed during the simple shear test. In this case too, there is a fine-grained region at a depth of 4 μm beneath the fracture surface. Further, the lamellar structure is preserved even at a distance of 4 μm from the fracture surface.

At this stage, it was not clear whether this fine-grained region developed prior to the propagation of the delamination crack upon the torsion test or simultaneously with the delamination crack. Fig. 3(b) shows several other cracks apart from the main delamination crack which is at the top. It should be noted that the microstructures around the cracks were also refined. The cracks extended to the middle of the fine-grained region. Fig. 3(d) shows a magnified image of the area near the delamination crack although the area is not the same as that in Fig. 3(b). The image shows the presence of fine-grained bands having a width of approximately 1 μm. These bands were not observed in the as-wire-drawn specimen, in both cross section and longitudinal section as can be seen from Fig. 3(a) and Fig. 1(c), respectively. Therefore, it can be surmised that the fine-grained region developed during the torsion test prior to delamination crack initiation and it grows during crack preparation. There are also several cracks near the delamination surface in Fig. 3(b). Although the surrounding areas of the cracks are expected also to have been ultra-fined, they were encroached by the ultra-fine region beneath the main crack. Although we will study this fine-grained region in detail in future works, it could be a type of shear band. It has been reported that shear bands develop in SUS 310S after cold rolling [14]. These shear bands formed owing to the destruction of the lamellar structure of the twin/matrix that was introduced. Further, fine grains developed in these shear bands. It was found that the lamellar structures of the shear bands underwent plastic deformation in the late stage of work hardening. In fact, shear bands have also been observed in a fully pearlitic steel after a tensile test at room temperature [9].

Fig. 4(a) and (b) shows bright field (BF) TEM images of areas far beneath the delamination crack and immediately beneath the delamination crack, respectively. Inclined cementite lamellae can be seen in Fig. 4(a). The black contrasts in the ferrite phase indicate the change in the orientation of the ferrite phase, suggesting that it underwent deformation during the torsion test. The selected area diffraction (SAD) pattern on the right at the bottom of the figure indicates that the BF image in (a) is from a single block. Fig. 4(b) shows that cementite lamellae cannot be seen clearly; however, faint contrasts nearly parallel to the cementite lamellae in Fig. 4(a) can be observed, indicating that the cementite lamellae had been dissolved. The dissolution of cementite in pearlitic steels has also been reported in specimens subjected to drawing and high-pressure torsion [6,15,16]. The SAD pattern in Fig. 4(b) tends to be ring-like patterns. It shows that grain size beneath the delamination crack became smaller and the ferrite orientation is deviating, which is in good agreement of IPF map shown in Fig. 3(e). The SAD pattern and microstructure shown in Fig. 4(b) are similar to those observed after a shear strain of more than 125 is applied by high-pressure torsion [15]. Although the value of strain in this study is not directly comparable with that in HPT in Ref. [15], the local severe plastic deformation should have taken place along the delamination crack. Since the ultra-fined region is approximately 4 μm thick, even a small amount of displacement induces a large value of shear strain. It is to be noted that it was found that such a large amount of plastic deformation for grain-refining took place immediately beneath the delamination crack.

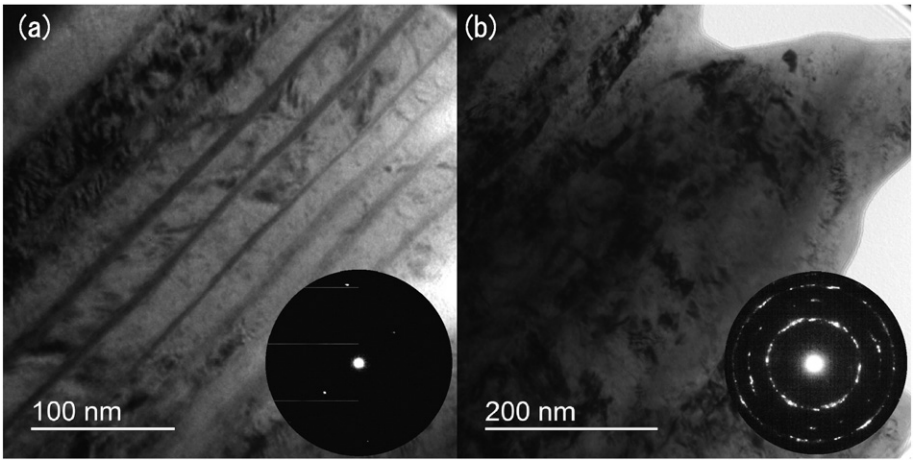

Fig. 4. (a) BF image of an area far from the delamination crack. (b) BF image of an area immediately beneath the delamination crack.

To conclude, in this study, a delamination crack was initiated along the longitudinal direction in a fully pearlitic drawn wire within one rotation during a torsion test. The fracture surface of the delamination crack was found to be completely different from the surfaces of brittle fractures. The microstructure of the area immediately beneath the delamination crack was investigated using SEM and TEM. Cementite lamellae were not observed immediately beneath the delamination crack. Further, just beneath the delamination crack, the microstructure consisted of fine grains. Finally, shear-band-like microstructures were observed near the delamination crack. It suggests that the small fine-grain regions were developed before the delamination crack propagates upon torsion test and the 4 μm-thick fine-grained region immediately beneath the delamination crack was developed during the delamination crack. Thus, it was concluded that delamination cracks are not brittle cracks nor simple ductile cracks but are attributable to the severe plastic deformation which is limited immediately beneath the crack.

Part of this work was supported by the Japan Science and Technology Agency (JST) under the Collaborative Research Based on Industrial Demand project named “Heterogeneous structure control: towards innovative development of metallic structural materials.”

References

[1] Y.J. Li, P. Choi, S. Goto, C. Borchers, D. Raabe, R. Kirchheim, Acta Mater. 60 (2012) 4005–4016.
[2] Y. Tomota, P. Lukas, D. Neov, S. Harjo, Y. Abe, Acta Mater. 51 (2003) 805–817.
[3] T. Ohashi, L. Roslan, K. Takahashi, T. Shimokawa, M. Tanaka, K. Higashida, Mater. Sci. Eng. A 588 (2013) 214–220.
[4] F. Danoix, D. Julien, X. Sauvage, J. Copreaux, Mater. Sci. Eng. A 250 (1998) 8–13.
[5] K. Hono, M. Ohnuma, M. Murayama, S. Nishida, A. Yoshie, T. Takahashi, Scr. Mater. 44 (2001) 977–983.
[6] J. Languillaume, G. Kapelski, B. Baudelet, Acta Mater. 45 (1997) 1201–1212.
[7] N. Maruyama, T. Tarui, H. Tashiro, Scr. Mater. 46 (2002) 599–603.
[8] G. Langford, Metall. Trans. 1 (1970) 465–477.
[9] M. Tanaka, Y. Yoshimi, K. Higashida, T. Shimokawa, T. Ohashi, Mater. Sci. Eng. A 590 (2014) 37–43.
[10] Y. Li, D. Raabe, M. Herbig, P.-P. Choi, S. Goto, A. Kostka, H. Yarita, C. Borchers, R. Kirchheim, Phys. Rev. Lett. 113 (2014) 106104.
[11] K. Shimizu, N. Kawabe, ISIJ Int. 41 (2001) 183–191.
[12] N. Nakada, N. Hirakawa, T. Tsuchiyama, S. Takaki, Scr. Mater. 57 (2007) 153–156.
[13] M.L. Martin, I.M. Robertson, P. Sofronis, Acta Mater. 59 (2011) 3680–3687.
[14] K. Higashida, T. Morikawa, Tetsu-to-Hagané 94 (2008) 576–581.
[15] Y. Ivanisenko, W. Lojkowski, R.Z. Valiev, H.J. Fecht, Acta Mater. 51 (2003) 5555–5570.
[16] Y.J. Li, P. Choi, C. Borchers, S. Westerkamp, S. Goto, D. Raabe, R. Kirchheim, Acta Mater. 59 (2011) 3965–3977.